

High-accuracy spectropolarimetric imaging using photoelastic modulator-based cameras with low-polarization coatings

Anna-Britt Mahler, Paula Smith, Russell Chipman, and Greg Smith
Optical Sciences Center, University of Arizona, Tucson, AZ 85721

Nasrat Raouf, Ab Davis, Bruce Hancock, Gary Gutt, and David J. Diner
Jet Propulsion Laboratory, California Institute of Technology, Pasadena, CA 91109

Abstract – Under NASA's Instrument Incubator Program (IIP), we are developing an electro-optical imaging approach to enable multiangle, multispectral, and polarimetric measurements of tropospheric aerosol column abundances and microphysical properties. From low Earth orbit, the measurements would be acquired from the ultraviolet to shortwave infrared at ~1 km spatial resolution over a broad swath. To achieve a degree of linear polarization (*DoLP*) uncertainty of 0.5% in several spectral bands, we temporally modulate the linear-polarization component of the light at a rapid rate, enabling each detector within a focal-plane array, combined with polarization analyzers, to measure the ratio of the linear Stokes components Q or U to the total intensity. Our system uses tandem photoelastic modulators (PEMs) within a reflective camera. Because the system must measure intensity in certain spectral bands and polarization in others, it is essential that the camera have low diattenuation, particularly in the intensity bands. We report on the status of our PEM-based camera concept, with particular emphasis on experimental and theoretical work to design a set of mirror coatings that minimize diattenuation over the range of spectral bands planned for the camera.

I. INTRODUCTION

Satellite remote sensing, by virtue of its global perspective, has a substantial role in measuring aerosol amounts and microphysical properties of importance to climate and air quality studies. Recent remote sensing advances have used a variety of approaches, each sensitive to different aspects of aerosol microphysics [1]. Passive multiangular, multispectral, and polarimetric sensing approaches each have unique strengths, and fusion of such capabilities in an imaging system would represent a major technological advance in our ability to monitor and characterize particulate matter from space. Polarization in particular has unique sensitivity to particle real refractive indices and widths of the particle size distributions [2]. Polarimetry in both the visible and shortwave infrared (SWIR) enables size-resolved retrievals of particle real refractive index. We envision an integrated spaceborne instrument that can provide multispectral and multiangular global coverage of the Earth in a few days. Furthermore, a degree of linear polarization (*DoLP*) uncertainty of 0.5% is specified within a subset of the spectral bands to provide accuracies required for climate-quality aerosol optical and microphysical property retrievals. We call this instrument concept the Multiangle SpectroPolarimetric Imager (MSPI), and the brassboard

instrument we are currently building is referred to as the Aerosol SpectroPolarimetric Camera (ASPC).

The starting point for definition of the MSPI instrument architecture is the Multi-angle Imaging SpectroRadiometer (MISR) instrument [3], currently in orbit on the Terra satellite. MISR acquires multiangle imagery in four visible/near-infrared bands from a set of nine pushbroom cameras, with the forward and backward viewing cameras paired in a symmetrical arrangement at a fixed set of view angles. A similar approach would be used for MSPI, though certain aspects of the MISR design require modification to accommodate the MSPI requirements. The optics must be capable of high transmission over a spectral range potentially as short as 355 nm and as long as 2130 nm. In addition to intensity measurements in multiple bands within this spectral interval, high-accuracy polarization measurements within a subset of the bands are also required, as noted above. Furthermore, the MSPI cameras are envisioned to have roughly twice the cross-track field of view of MISR.

The MISR pushbroom cameras acquire multispectral, non-polarimetric observations using focal planes in which adjacent line arrays are overlain by filters passing different wavelengths [3]. The analog of this measurement approach for polarimetry would be to overlay different line arrays with analyzers in different orientations. MISR experience shows that the data from different lines within a single camera can be digitally co-registered to better than 1/10 of a pixel; however, even after extensive analysis residual uncertainties in the radiometric cross-calibration between channels are on the order of 1-2%. Such an arrangement would by itself risk violating the 0.5% *DoLP* requirement, and some additional means of reducing errors is needed.

Under NASA's Instrument Incubator Program (IIP), we are building a brassboard spectropolarimetric camera that incorporates a dual photoelastic modulator (PEM) imaging approach to temporally modulate the linear-polarization component of incoming light at a sub-pixel rate, enabling each detector within a focal-plane array, combined with polarization analyzers, to measure the relative proportions of the linear Stokes components to the total intensity. This design circumvents inaccuracies introduced by detector gain changes or uncertainties in flight that could compromise meeting the required *DoLP* accuracy with a static detection approach. Our "self-calibrating" system uses tandem

photoelastic modulators (PEMs) in a camera with reflective optics having high-reflectance, low diattenuation mirrors. The approach is spectrally versatile, and can benefit other applications besides aerosol remote sensing.

II. PROJECT STATUS

A. Optical design and fabrication

The ASPC optical design is a three-mirror reflective off-axis anastigmatic design suitable for the dual-PEM-based spectropolarimetric camera. The required $\pm 31^\circ$ FOV is accomplished by using a convex spherical primary mirror. The aspheric secondary and tertiary mirrors create a long region in the optical path where the rays from any point in the FOV are nearly collimated. The PEMs (along with two quarter-wave plates which are required so that Q and U are modulated) are placed in this region, immediately before and after the system stop, and are tilted at a small angle to the optical axis to avoid ghost images at the image plane. An $f/5.6$ focal ratio is chosen to balance light throughput requirements and the need to limit the angle of the cone of light passing through the filters and polarizers mounted above the focal plane line arrays. To minimize variation in spectral response across the FOV, the chief rays from different points in the field are telecentric in the image plane, traversing the interference filters at nearly the same angle. A ray-trace diagram of the optical design is shown in Fig. 1. This illustration shows a design with an effective focal length (EFL) of 29-mm, which when matched with focal plane pixels of $10\ \mu\text{m}$ pitch provides a nadir resolution of 7 m from a 20-km altitude and 225 m from 650 km. Spot sizes across the FOV were kept below $10\ \mu\text{m}$ in diameter by careful optimization of the mirror asphere parameters. An achromatic (650 and 1610 nm) $1/4\text{-}\lambda$ retarder design is also complete.

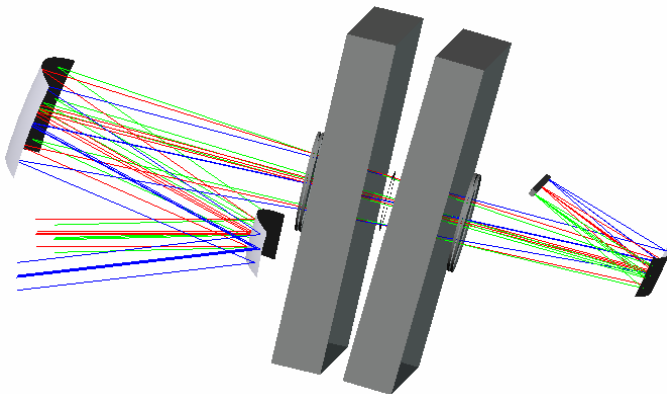


Figure 1. View of a three-mirror camera design with an integrated dual-PEM retarder. The PEMs have a small wedge angle between them to minimize ghosting.

Four sets of mirror 1 and three sets of mirrors 2 and 3 were procured under the IIP, and all are ready to be coated. The first set is being used for the laboratory brassboard, and will be coated when the coating design stage is complete. We hope to use the second set in a camera suitable for airborne observations. Optical testing shows that all mirrors were fabricated within specification.

B. Mechanical design and fabrication

The ASPC mechanical assembly is comprised of a base, three mirror mounts, a dual PEM assembly, a focal plane, and a set stray light baffles (see Fig. 2). The base provides structural support for all elements of the camera and interfaces to a gimbal. Parallel rods attach to the base, provide accurate spacing and stability for the 5 mounts (for mirror 1, mirror 2, the dual PEM assembly, mirror 3, and the focal plane). A protective cover (not shown) is placed over the assembly.

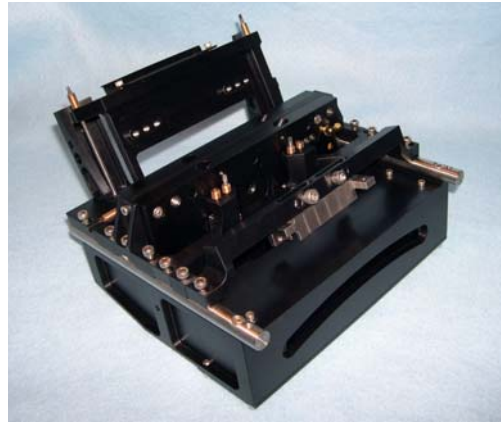


Figure 2. ASPC mechanical assembly, including the dual PEM assembly. M2 mirror mount and protective cover (not shown).

A tolerance analysis on the optical design was performed in order to understand the degrees of freedom needed to align the system, and to determine the requirements on positional accuracy for the mechanical assembly. The result of this analysis is that mirrors are mounted on flexural supports and have provisions for fine alignment including:

- (1) 2 degrees of freedom (dof) on mirror 1; decenters in x and y .
- (2) Spacing between mirror 1 and mirror 2; mirror 2 translates in z .
- (3) 5 dof on mirror 2; tilt about x , y and z , and translation in x and y .
- (4) Spacing between mirror 2 and mirror 3; mirror 2 translates by various coupled dofs.

- (5) 0 dof on mirror 3; this mirror will be fixed.
- (6) 3 dof on the FPA; tilt about x and y and translation in z.

The mechanical design places optical elements in their theoretical location to within tilts of 15 arcmin, decenters of 0.1 mm and element spacings of 0.1 mm. All parts are made of anodized aluminum except the rods and mirror cells, which are invar. Two mechanical assemblies were fabricated, one is assembled and shown in Fig. 2. The mechanical design also accommodates 3 separate focal plane configurations to aid in our 3 step alignment, which will begin once the mirrors have been coated.

C. Dual PEM assembly

The dual PEM assembly was tested for power dissipation, thermal, and structural integrity. As a result, this element of the camera has moved from technology readiness level 3 (TRL-3) to TRL-5. The PEM is now operating at 1.25x the planned retardance amplitude for the flight system. This room-temperature life test will be continued indefinitely.

D. Test equipment

To test the ability of the ASPC to meet the 0.5% *DoLP* accuracy requirement, the University of Arizona polarization laboratory designed and built a precision Polarization State Generator (PSG). The PSG is designed to simulate weakly polarized states with degree of polarization ranging from 0 to 0.19. In the PSG, a light pipe scrambles the input polarization to create a completely depolarized beam. Reflection from a glass plate then produces a degree of polarization that is controlled by motorized adjustments of the angle between the glass plate and the beam. To generate the complete range of weakly polarized states, calibrated retarders are used to set the orientation and ellipticity of the polarization exiting from the PSG. Fabrication of the PSG is complete, and precision calibration is in progress.

IV. LOW DIATTENUATION MIRROR COATINGS

A. Coating design considerations

The mirror coatings must satisfy several simultaneous requirements. First, a diattenuation specification of $< 1\%$ is established so that cameras can operate as high-accuracy intensity imagers in the non-polarization bands (the total intensity uncertainty requirement is 3%, of which diattenuation is one component of the error budget). The diattenuation requirement can be relaxed at those wavelengths where polarization measurements will be taken, because diattenuation can be measured in these channels and thus diattenuation effects can be removed in calibration. Second, high reflectivity over a broad wavelength range is needed to provide good signal-to-noise ratio. Third, coating

retardances should be close to a half-wave of retardance in the polarization bands to prevent the coupling of circular into linear polarization, though this is a relatively minor issue given that natural scenes have little circular polarization.

Diattenuation is defined as $D = \frac{|R_s - R_p|}{R_s + R_p}$, where R_s and

R_p are reflectivities for s-polarization (vertical) and p-polarization (horizontal) specified in the Fresnel equations. Thus, in order to keep diattenuation low, the difference between R_s and R_p must be very small at the focal plane. Upon reflection from an uncoated metal mirror, R_s is typically greater than R_p . The MSPI thin film coatings have been designed such that this typical relationship between R_s and R_p upon reflection from a mirror is reversed at many wavelengths.

For simplicity, we assume that horizontal/vertical diattenuation is the only type present, and use positive values to denote horizontal diattenuation while negative values denote vertical diattenuation. In this way, diattenuation cancellation can occur by summing the positive and negative values from the three coatings at all wavelengths. More accurate analysis of coating performance at the actual angles of incidence experienced by each ray can be obtained from polarization raytracing. Polarization raytrace analysis results will be discussed in subsection D.

B. Coating layer index determination

To optimize the coating designs, witness samples of test coatings were measured in the University of Arizona (UA) Mueller Matrix Imaging Polarimeter (MMIP). The University of Arizona ellipsometrically determined thicknesses and refractive indices of actual coatings and obtained measured values of diattenuation, reflectance and retardance.

The MMIP, shown in Fig. 3, acquires Mueller matrix images of dimensions 99 pixels by 99 pixels. To construct the Mueller matrix, a series of snapshot images are sequentially captured while retarders in the polarization state generator and polarization state analyzer arms step through a series of angles in a 5-to-1 ratio. Data analysis software reduces the irradiance images to construct Mueller matrix images, with 30x averaging to improve signal-to-noise. A monochromator source provides wavelength tunability from 400 nm to 800 nm. Precision is approximately 0.1% for diattenuation and 0.8° for retardance. A repeatability study is currently underway to understand overall measurement uncertainty.

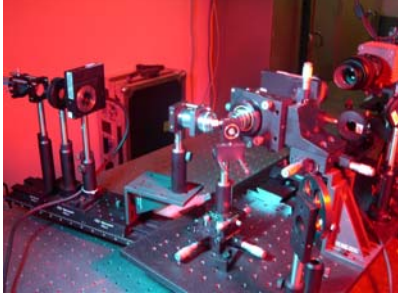


Figure 3. University of Arizona Mueller matrix imaging polarimeter (MMIP). From left to right, the system consists of a polarization state generator (a tunable monochromatic source, a collimating lens, polarizer, and rotating retarder), microscope objectives (optional), sample, a polarization state analyzer (rotating retarder, polarizer), and a CCD camera.

Mueller matrix images of witness samples were obtained at angles varying from 14° to 60° . Diattenuation and reflectance data obtained from UA MMIP measurements did not agree well with modeled data for the test coatings, so least-squares fitting was performed to find coatings that would match the measured data. The real and imaginary parts of the index of refraction were varied for the top 4 layers along with their thicknesses. The index values (for both n and k) were allowed to vary according to $n_{\text{optimized}} = n_{\text{initial}} + c + \frac{d}{\lambda}$, where c and d are constants. The merit functions used include RMS error in diattenuation, reflectance, and a combination of the two. Choice of merit function at any given stage of the fitting process was determined by qualitative assessment of performance. Retardance values were not significantly different between the measured and modeled data and were not included in the merit function.

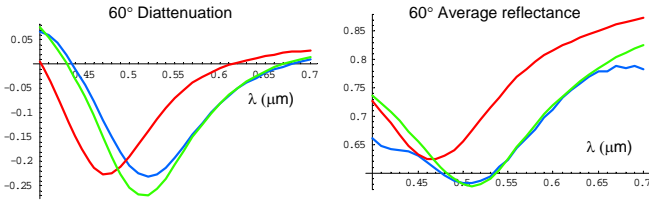


Figure 4. Diattenuation and average reflectance data vs. wavelength (mm) for the initial modeled index values (red), the UA MMIP measured index values (blue), and the UA index values giving the best agreement with the measured data (green) at 60° angle of incidence.

Fig. 4 shows plots of diattenuation and reflectance with the original modeled data, the measured data and the data of the modeled coating that best matched the measured data. Results of this fitting process showed that best matches to measured data were found if index values were altered, not just thicknesses, indicating that thicknesses alone were not responsible for the mismatch. Index values used for initial design were obtained from relatively thick coating layers. One possible explanation for the mismatch is that these

materials behave differently in thin stacks due to interactions at layer boundaries.

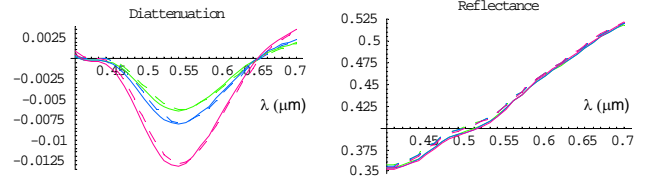


Figure 5. Diattenuation and average reflectance values vs. wavelength (μm) for the on-axis (green), 15° (blue) and 31° (pink) fields. Solid lines indicate values from UA determined indices, dashed lines indicate values from Woollam, Inc. determined indices. The plots show that these data give similar results across a wide range of wavelengths.

To better understand the materials in our design, single-layer coatings provided by Surface Optics Co. were independently ellipsometrically characterized by Woollam Inc. The index values obtained by Woollam Inc. were used in our thin film model, and diattenuations and reflectances obtained using these data were similar to those obtained using the optimized index values, as shown in Fig. 5. This independent analysis of test coatings provided sufficient confidence in our new coating index values that a combination of these index data were used to design new diattenuation cancellation coatings.

C. Coating design optimization

Using the average of the index values determined by UA and by Woollam Inc., a set of coatings were designed that are optimized for low combined diattenuation and high reflectance. The merit function used for these coatings is as follows:

$$200\left(2\sum_1|D| + \sum_2|D|\right) + \left(2\sum_1(1-R) + \sum_2(1-R)\right),$$

where D is diattenuation, R is average reflectance, \sum_1 indicates the sum of the values at wavelengths between 400 nm and 500 nm, and \sum_2 indicates the sum of the values at wavelengths between 510 nm and 700 nm. This merit function weighs diattenuation and reflectance approximately equally given the actual values of diattenuation and reflectance in these coatings. Shorter wavelengths are weighted more heavily because experience showed that diattenuation is more difficult to control at shorter wavelengths. Our current 4 best designs of 3-mirror coating combinations, optimized using this merit function, are shown in Fig. 6. The $< 1\%$ diattenuation requirement is met at all wavelengths except 355 nm, where the value is 1% for the on-axis field and 2% for the 31° field. Finite difference analyses of coating thicknesses and indices have furthered our understanding of the tolerances we can expect from our current coating model. They suggest that we are moderately

sensitive to thickness and index variations in layers 1 and 2, and we are most sensitive to thickness and index variations in layer 3.

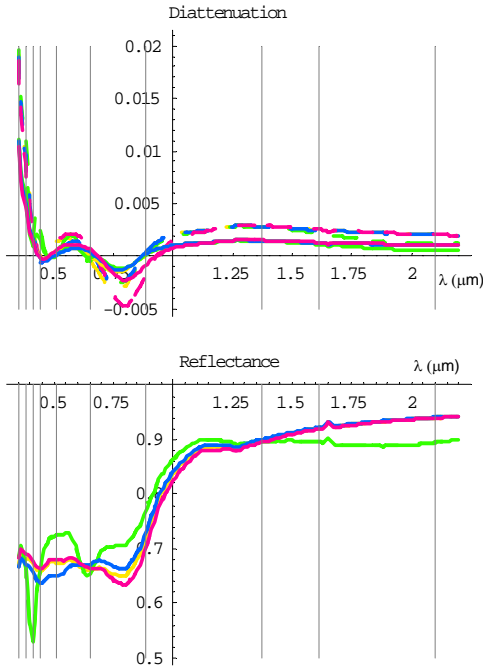


Figure 6. Diattenuation and average reflectance of current best 4 3-mirror coating design combinations. Different designs are shown in different colors. Solid indicates on-axis field, dotted indicates 31° field.

D. Polarization raytrace analysis

The multilayer thin film model used in the preceding analysis is very effective for understanding one ray at a time. However, a full raytrace analysis allows us to characterize the polarization performance of the coatings given the actual angles of incidence that each ray will be experiencing.

Code V was used to perform raytrace analysis on the MSPI camera. This model considers the effects of mirror coatings, anti-reflection (AR) coatings on the waveplates and PEMs, birefringence of the quartz/sapphire waveplates and fused silica PEMs, in addition to the angles of incidence experienced by each ray at every surface.

For the current coating model, baseline AR coatings, and with the dual PEM assembly turned off (i.e., non-modulating), plots of RMS diattenuation across the pupil are shown as a function of wavelength the on-axis field (Fig. 7) and the full field (Fig. 8). Currently, the diattenuation specification is met for all wavelengths in the on-axis field, but not for the full field.

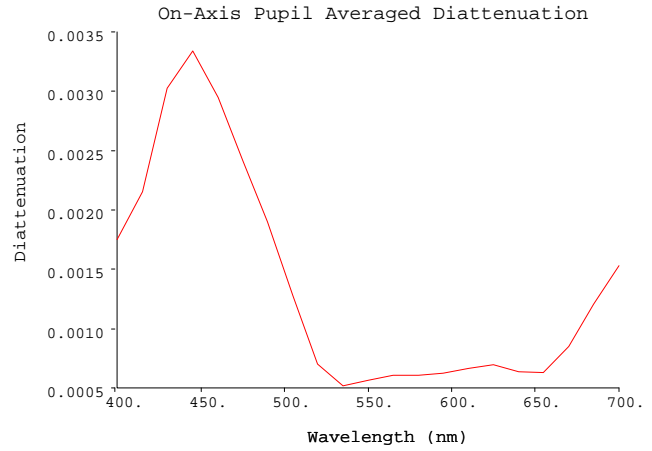


Figure 7. Pupil averaged diattenuation vs. wavelength (nm) for the on-axis field. The diattenuation requirement has been met at all wavelengths for this field.

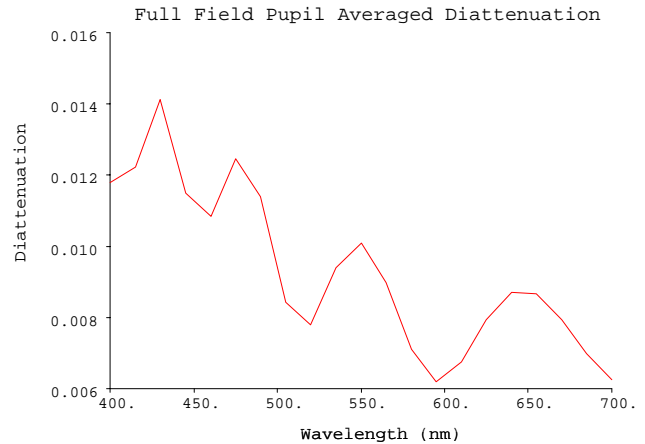


Figure 8. Pupil averaged diattenuation vs. wavelength (nm) for the full field. The diattenuation requirement is not yet met at all wavelengths for this field.

E. Effects of the PEMs on diattenuation

The raytrace analysis furthers our understanding of the system by combining the effects of the many rays our system is experiencing. However, this analysis was done assuming that the dual PEM assembly was turned off. Once the dual PEM assembly is turned on, it acts as a time-dependent circular retarder, and diattenuation entering the dual PEM assembly will exit with an altered diattenuation. Initial results indicate that it may be advantageous to find the combination of two coatings that minimizes diattenuation for mirrors 1 and 2, and a third coating that minimizes diattenuation for the incidence angles experienced by mirror

3. Additional modeling and raytrace analysis is being performed to investigate this further.

V. SUMMARY AND STATUS

The dual-PEM polarimetric imaging approach is maturing under the IIP. Practical designs for key elements of the high-reflectance low-diattenuation optical system are in progress and detailed analysis of the flight system architecture is underway. The diattenuation cancellation coating design capability has been demonstrated over a broad bandwidth. The ASPC will demonstrate technology needed to incorporate the MSPI instrument into a next-generation Earth-orbiting aerosol mission.

ACKNOWLEDGMENTS

This research was carried out, in part, at the Jet Propulsion Laboratory, California Institute of Technology, under contract with the National Aeronautics and Space Administration. Work at the University of Arizona College of Optical Sciences is supported by a JPL subcontract.

REFERENCES

- [1] Yu, H., Y.J. Kaufman, M. Chin, G. Feingold, L.A. Remer, T.L. Anderson, Y. Balkanski, N. Bellouin, O. Boucher, S. Christopher, P. DeCola, R. Kahn, D. Koch, N. Loeb, M. S. Reddy, M. Schulz, T. Takemura, M. Zhou, "A review of measurement-based assessments of the aerosol direct radiative effect and forcing," *Atmos. Chem. Phys.* **6**, 613-666, 2006.
- [2] Mishchenko, M.I. and L.D. Travis, "Satellite retrieval of aerosol properties over the ocean using polarization as well as intensity of reflected sunlight," *J. Geophys. Res.* **102**, 16989-17014, 1997.
- [3] Diner, D.J., J.C. Beckert, T.H. Reilly, C.J. Bruegge, J.E. Conel, R.A. Kahn, J.V. Martonchik, T.P. Ackerman, R. Davies, S.A.W. Gerstl, H.R. Gordon, J-P. Muller, R.B. Myneni, P.J. Sellers, B. Pinty, and M. Verstraete, "Multi-angle Imaging SpectroRadiometer (MISR) instrument description and experiment overview," *IEEE Trans. Geosci. Rem. Sens.* **36**, 1072-1087, 1998.